PCCP

Accepted Manuscript

ROYAL SOCIETY OF CHEMISTRY

www.rsc.org/pccp

Journal Name

ARTICLE

Evaporation-Induced Self-Structuring of Organised Silica Nanohybrid Films Through Cooperative Physical and Chemical Interactions

Received 00th January 20xx,
Accepted 00th January 20xx

DOI: 10.1039/x0xx00000x

www.rsc.org/

Ana M. Cojocariu[a,b,c], Xavier Cattoën[b,d,e,*], Rozenn Le Parc[f], David Maurin[f], Christophe Blanc[f], Philippe Dieudonné[f], Jean-Louis Bantignies[f,*], Michel Wong Chi Man[b], and John R. Bartlett[a,c,*]

In this work, we develop the concept of evaporation-induced self-structuring as a novel approach for producing organised films by exploiting cooperative physical and chemical interactions under far-from-equilibrium conditions (spin-coating), using sol-gel precursors with multiple functional groups. Thin films of self-structured silsesquioxane nanohybrids have been deposited by spin coating through the sol-gel hydrolysis and condensation of a bridged organosilane bearing self-assembling urea groups. The resulting nanostructure, investigated by FTIR, AFM and SEM, is shown to be highly dependent on the catalyst used (nucleophilic or acidic), and can be further modulated by varying the spinning rate. FTIR studies revealed the presence of highly organized structures under acidic catalysis due to strong hydrogen bonding between urea groups and hydrophobic interactions between long alkylene chains. The preferential orientation of the urea cross-links parallel to the substrate is shown using polarized FTIR experiments.

Introduction

Over the past decade, significant effort has been directed towards the elucidation of synthesis/structure/function correlations to guide the development of synthetic strategies for controlling the composition, size and shape of nanomaterials. In this context, organic-inorganic nanohybrids incorporating bridged silsesquioxanes have been of particular interest, due to their versatility and the structural control that can be achieved through independent modulation of the properties of the organic bridge and inorganic moieties.[1-3] Such strategies have also been applied to the production of thin films on a variety of substrates, driven by the continuing need to develop new and enhanced materials with nanostructures engineered over multiple length scales for applications in electronics, optics, sensing, ferromagnetics, shape-selective membranes, etc.[4-11] New approaches and insights into the mechanisms that control the morphology of such thin films, including the development of structure/function correlations, are required to better control their properties and open up new applications for these materials.[11-13]

A particularly versatile approach for achieving controlled organisation in bridged silsesquioxanes involves the use of organic bridges that are capable of playing a structure-directing role through non-covalent interactions such as H-bonding,[14] hydrophobic interactions,[15] pi-pi stacking,[16] van der Waals forces,[17] etc. Combining such strategies with thin-film deposition techniques such as dip- or spin-coating opens up the possibility of using a combination of chemical and physical interactions to achieve patterning in thin films over multiple length scales.[18] We have previously demonstrated this approach in conjunction with an enantiomerically pure bis-silylated (1R,2R) diureidocyclohexane compound, to prepare thin films with a hierarchical structure.[19] Depending on the processing conditions used, both patterned fibrous morphologies and uniform, interconnected nanoparticles could be readily produced through careful manipulation of the physical and chemical processing parameters. Complementary strategies involving the use of external templating agents such as surfactants, combined with evaporation-induced self-assembly (EISA) during dip-coating, have also been used to produce a range of materials with ordered mesoporosity that incorporate functional organic species.[4]

Despite the rich palette of precursors that have now been described, and the mechanistic insights that have been reported in bulk systems, few studies have exploited cooperative physical and chemical control in spin-coating to modulate self-structuring in the absence of external templating species such as surfactants.[19] Spin coating in such complex systems is a highly non-equilibrium process, with

[a] Faculty of Science, Health, Education and Engineering, University of the Sunshine Coast, Maroochydore DC, QLD 4558, Australia. JBartlett@usc.edu.au
[b] Institut Charles Gerhardt Montpellier, UMR 5253 ENSCM-Université Montpellier-CNRS, 8, rue de l'école normale, 34296 Montpellier, France.
[c] School of Science and Health, University of Western Sydney, Locked Bag 1797, Penrith, NSW 2751, Australia.
[d] CNRS Inst. Néel, F-38042 Grenoble, France. xavier.cattoen@neel.cnrs.fr
[e] Univ. Grenoble Alpes, Inst. Néel, F-38042 Grenoble, France.
[f] Laboratoire Charles Coulomb (UMR CNRS 5521), Université Montpellier 2, 34095 Montpellier Cedex 5, France. Jean-Louis.Bantignies@univ-montp2.fr
† Electronic Supplementary Information (ESI) available: [Additional figures and table]. See DOI: 10.1039/x0xx00000x

rapid increases in reactant concentration during solution spreading and evaporation (induced by substrate spinning) interacting with nucleation, growth, self-structuring and polycondensation processes during formation of the coating. A particular feature of such coupled systems is that the time available for solution species to diffuse and react during coating deposition is short, and non-equilibrium structures would be expected to be "frozen" in place. This interplay between physical and chemical processing parameters, particularly in cases where self-structuring of the precursor can occur during solvent evaporation induced by the spin-coating process, would be expected to provide new and novel approaches to controlling the molecular architecture and nanostructure of thin films, together with their associated optical and surface properties.[12, 13]

In this paper, we describe the preparation of thin films via an evaporation-induced self-structuring approach using a bridged organosilane (1,12-Bis[(triethoxysilyl)propyl-ureido]dodecane) (Scheme 1) that incorporates an organic bridge containing urea moieties separated by a dodecyl chain. The influence of key chemical (particularly pH and ageing time) and physical parameters (spinning speed) on the morphology of the resulting coatings is elucidated, and a model describing the structural evolutions of the coatings is developed as a general approach for producing self-structured coatings under far-from-equilibrium conditions.

Experimental

Preparation of sols

The synthesis of **P12** (1,12-bis[(triethoxysilyl)propylureido] dodecane, $C_{32}H_{70}O_8N_4Si_2$, formula weight 695, Scheme 1) has been described previously.[20] The precursor is sensitive to moisture, and hence it was synthesised and stored under an inert atmosphere.

The sols were prepared (Scheme 1) by dissolving **P12** (50 mg) in 1-propanol (5 g). To initiate the hydrolysis and condensation reactions, a mixture of water and catalyst was added (10.4 mg). The solvent (1-propanol) also contained 0.4 % H_2O (Karl Fischer analysis), which was taken into account in the calculations of the sol composition (resulting in a total Si:H_2O molar ratio of 1:23). Three types of catalysts were investigated: acidic (HCl, pH = 2), nucleophilic (NH_4F, 1M) and basic (NH_4OH, pH = 11). The sols were aged for 1 to 24 h and filtered using 0.2 µm PTFE filters prior to their use in coating experiments.

Deposition of films

Coatings were deposited on polished (100)-oriented silicon wafers (Neyco, Type P with B dopant, IR quality, 2'' diameter x 280 µm thick) and glass slides (Schott Borofloat®) from the sols via spin-coating (G3-8 spin coater from Specialty Coating Systems) in an open atmosphere. Prior to coating, the glass slides were cleaned in piranha solution and the silicon wafers were cleaned using the RCA 1/2 protocol.[21] Comparable results were obtained using both types of substrates. The clean substrates were dried by spinning for 60 s at 8000 rpm. Using a syringe, two drops of the sol were deposited on the centre of the substrate and coatings were formed by spinning for 60 s at 1000, 3000, 5000 or 8000 rpm, with an acceleration/deceleration time of 10 s. The resulting films were dried at ambient temperature for 24 h and then at 60 °C overnight. Leaching studies were subsequently performed via Soxhlet extraction in refluxing ethanol to ensure that no unreacted **P12** remained in the dried coatings.

Reference bulk material

A reference bulk material was synthesized under acidic catalysis using the following conditions: pH ~ 2; concentration, 1 wt% **P12** in 1-propanol; ageing time, 72 hours; mole ratio **P12**:HCl:H_2O:1-PrOH, 1:0.0054:45:1152. The powder was collected by centrifugation, washed with water and then ethanol and dried at 60 °C overnight. This sol contained three times more catalyst than the acidic sol used for the coatings in order to initiate the condensation.

Characterisation

Dynamic light scattering (DLS) was used to probe the initial stages of nucleation and growth in the sols immediately after addition of the aqueous HCl or NH_4F catalyst solutions to the P12 solution. Following addition of the catalyst, the solutions were immediately filtered using 0.2 µm Millipore filters and DLS measurements were subsequently performed using an AMTEC goniometer equipped with a Brookhaven BI9000-AT correlator and an Ar^+ laser operating at 514.5 nm. All experiments were performed at a scattering angle of 90°. The autocorrelation data were fitted with a single exponential function to derive the hydrodynamic radii of the scattering species. The evolution of hydrolysis and condensation products in the HCl-catalysed system was further probed using electrospray mass spectroscopy (Waters Corporation Synapt G2-S). The sols were diluted by a factor of 100 in acetonitrile prior to injection. The positive electrospray ionisation experiments were conducted using a capillary potential of 1.2 kV and a cone potential of 30 V.

Scanning electron micrographs (SEM) of the coated samples were obtained using a Hitachi S-4800. All samples were coated with platinum prior to analysis. The surface morphology of the coatings was investigated via atomic force microscopy, in tapping mode, using a NanoMan AFM (Bruker Instruments) equipped with a Nanoscope V controller and NanoSensor tips or on a Veeco D3100 with a Nanoscope V controller using Olympus AC160 tips. The typical scan size was 10 × 10 µm^2.

Attenuated total reflection infrared absorbance spectra (FTIR-ATR), using either diamond (3000 -1300 cm^{-1}) or silicon wafer (1300 – 800 cm^{-1}) as waveguides, were recorded using a Bruker IFS 66V spectrometer equipped with a liquid N_2-cooled MCT detector. Spectra were collected from 600 to 4000 cm^{-1} at a resolution of 4 cm^{-1}, and 512 scans were co-added for each spectrum. To identify the underlying spectral components within complex peak profiles observed in the

spectra, PeakFit software (supplied by Systat) was used to fit Gaussian-Lorentz curves to the band profiles.

The thickness of the coatings was determined by scratching the coatings with a glass slide and then measuring the size of the resulting step with a TENCOR Alpha-Step IQ profilometer. At least three measurements were performed in each case over a distance of 1000 µm at 20 µm s^{-1} scan speed and 0.4 µm horizontal resolution.

Results and Discussion

A number of studies have elucidated the various chemical processes occurring during the conversion of bridged organosilanes into bulk gels and the effect of processing parameters such as pH, alkoxide group, solvent, catalyst, reactant concentrations and the nature of the bridge have been described.[17, 20, 22-24] The structure of the products obtained is particularly sensitive to the properties of the bridging group, as expected. For example, studies of a homologous series of alkylene-bridged silsesquioxanes have revealed that even small changes in the length of the bridging chains can have a profound influence on the gelation kinetics in such systems.[25] Bantignies et al demonstrated that ordered lamella structures could be obtained in such systems when the bridging organic species contained two urea groups separated by a long alkylene chain.[17] In this case, self-structuring within the resulting gels was controlled by hydrophobic interactions between adjacent alkylene chains coupled with H-bonding interactions between urea species. The number of methylene units within the alkylene chain was found to play a key role, with the degree of structural order being modulated by both the length and parity (i.e. odd or even number of methylene groups) within the alkylene chain.

As discussed in our earlier studies,[19] a particular challenge associated with the use of multifunctional precursors such as **P12** for the deposition of thin films is to identify the processing window (pH, precursor concentration, ageing time, spinning speed, etc) that yields uniform, adherent coatings. The results of an extensive parametric study indicated that continuous, uniform and adherent coatings could only be obtained under HCl-, NH_4F- and NH_4OH- catalysed conditions using a narrow range of processing parameters:

- Acid-catalysed (HCl) conditions: pH ~ 2; concentration, 1 wt% **P12** in 1-propanol; ageing time, 1 to 24 hours; spinning speed, 1000 to 8000 min^{-1}; mole ratio **P12**:HCl:H_2O:1-PrOH, 1:0.0014:23:1152;
- Fluoride-catalysed (NH_4F) conditions: concentration, 1 wt% **P12** in 1-propanol; ageing time, 1 to 24 hours; spinning speed, 1000 to 8000 min^{-1}; **P12**:NH_4F:H_2O:1-PrOH, 1:0.14:23:1152;
- Base-catalysed (NH_4OH): pH ~ 11; concentration, 1 wt% P12 in 1-propanol; ageing time 1 to 24; spinning speed 1000 to 8000 min^{-1}; **P12**:NH_4OH:H_2O:1-PrOH, 1:0.0081:23:1152

In particular, the use of 1-propanol as solvent was found to be crucial for producing uniform coatings, due to the low solubility of **P12** in other solvents. Low-angle XRD data obtained from powders produced in 1-propanol under HCl-catalysed conditions confirmed that the expected lamellar structure was present, with patterns similar to those observed in our earlier studies being obtained (Figure S1, Supporting Information).

The structural evolution of the coating sols, and the conditions under which high-quality coatings can be obtained within these processing windows, are discussed in detail below.

Nanoscale Structure of Coatings

The macroscopic structure of the coatings obtained from HCl-, NH_4F- and NH_4OH-catalysed coating sols aged for four hours prior to deposition is illustrated in Figure S2. Distinctly different morphologies are evident, with the HCl-catalysed system exhibiting nanoscale patterning (due presumably to self-assembly, as described below) while the NH_4F-catalysed system is smooth on the length scales probed by SEM. Coating striations are evident in the case of the NH_4OH-catalysed system, and in general, these latter coatings were of low quality irrespective of the processing conditions used. FTIR studies (Figure S3, Supplementary Information) also revealed that hydrolysis and condensation were not complete in the case of coatings produced from the NH_4OH-catalysed system and hence, this system will not be addressed further in the current study.

The significant differences in the morphology of the coatings produced from HCl- and NH_4F-catalysed sols are further evidenced from their respective AFM micrographs, which are illustrated in Figure 1. This comparison clearly highlights the nanoscale patterning obtained in the case of HCl-catalysed sols and the lack of any such patterning in the case of the NH_4F-catalysed system. The former system exhibits a uniform fibrous morphology, with the fibres arranged in a "net-like" structure with relatively uniform holes. Higher resolution AFM data (Figure S4, Supplementary Information) reveal that the fibres are composed of bundles of smaller fibres with diameters of less than 50 nm. As expected, the value of the roughness (R_a) measured for the NH_4F-catalysed system (0.8 nm) is substantially lower than the corresponding value for the HCl-catalysed system (3 to 9 nm). The morphology of the coatings deposited from the HCl-catalysed sols is also significantly influenced by the spinning speed used during deposition (Figure 2), with increasing speed leading to a corresponding decrease in the nanoscale roughness, the average length of the fibres and the size of the holes in the net-like structures. As expected, the overall thickness of the coatings exhibited a power-law dependence on increasing spinning speed (Figure S5), although the power-law exponent (-0.4) is different to the expected value (-0.5),[26] due presumably to a non-Newtonian rheology in the coating solution.

There have been only a small number of reports describing the deposition of patterned coatings from bridged organosilanes containing structure-directing moieties,[19, 27] and it is of interest to compare the morphology of the coatings deposited in this work with those reported in earlier studies. Karatchevtseva et

al obtained patterned morphologies controlled on multiple length scales using a chiral BS (bis-silylated (1R,2R) diureidocyclohexane), with a uniform fibrous morphology obtained under base-catalysed conditions (attributed to self-assembly) and a morphology based on the clustering of spherical nanoparticles evident in the case of acid-catalysed conditions.[19] In addition, control of structure was achieved on multiple length scales, with the dimensions of the nanosized "building blocks" controlled via ageing time in solution and their assembly into organised structures controlled via the spin-coating speed. As demonstrated in the following Section, ageing in solution in the case of the HCl-catalysed system used in the current work has essentially no impact on the size of the building blocks, due to the absence of inorganic polycondensation.

Molecular-Scale Evolution of Coating Solutions

In view of the narrow range of coatings conditions that were identified in the preliminary scoping studies for producing high-quality coatings, the evolution of the coating solutions with time was investigated for both HCl- and NH_4F-catalysed conditions. The results of a DLS study of the hydrodynamic radii of species formed in the solutions as a function of ageing time is illustrated in Figure 3. A monotonic increase in the hydrodynamic radius in the NH_4F-catalysed system is clearly observed, with 3-5 nm particles observed after ageing for 24 hours. In contrast, no evolution in the sols produced in the HCl-catalysed system is evident for ageing times of up to 24 hours, with no scattering species larger than the detection limit of the DLS experiment observed (< 1 nm[28] assuming a viscosity equivalent to that of the pure solvent).

Previous studies have demonstrated that mass spectrometry can also provide significant insights into the evolution of species in sol-gel solutions after hydrolysis is initiated,[29, 30] and hence the evolution in the HCl-catalysed system was further probed by electrospray mass spectrometry (Figure S6). In general, the **P12** precursor (formula weight M = 695) is observed either in its protonated (M = 696) or Na^+-**P12** adduct form (M = 718). The loss of an EtOH molecule from the protonated H^+-**P12** is also evident from the peak at M = 650, which presumably occurs during the electrospray process. Minor quantities of heavier products are also found at M = 1413 (corresponding to Na^+-2**P12**), reflecting the propensity of **P12** to self-assemble via H-bonding even under the dilute conditions used in the ESI experiment. Further peaks clustered around M = 1413 are assigned to partly hydrolysed species (loss of ethoxide, M = (1413-28)), partial transesterification (M = 1413+14), etc. However, no significant condensation is evident, as reflected by the lack of peaks associated with polycondensed species with masses exceeding 1500 after 24 hours of ageing. This observation is entirely consistent with the findings of the DLS experiment. The evolution of a complex series of peaks with ageing time at masses less than M = 718 reflects the progress of hydrolysis and transesterification reactions in the system, confirming that hydrolysis and condensation are essentially decoupled in this system under acid-catalysed conditions.

It is also interesting to note that many of the peaks clustered around M = 718 and M = 1413 in the ESI data can be represented by the following simple rules:

- $M = 1413 \pm 14n$
- $M = 718 \pm 14n$

where n = 0,1,2,3, etc. This is consistent with the evolution outlined above:

- Transesterification, i.e. replacement of Et species with Pr (from the solvent), and the associated formal addition of a CH_2 group, leading to a net mass increase of 14 for each transesterification event;
- Hydrolysis, i.e. conversion of Et-O-Si≡ species to EtOH and HO-Si≡, with an associated net mass loss of 28 for each ethoxy ligand hydrolysed;
- Transesterification followed by hydrolysis at the same site, i.e. the initial replacement of Et with Pr (net mass increase of 14), followed by conversion of Pr-O-Si≡ to Pr-OH and HO-Si≡ (net mass loss of 42). In this case, the overall mass loss is 28 for each transesterification/hydrolysis event;
- Transesterification at one site (net mass increase of 14) and hydrolysis at another site on the precursor molecule (net mass loss of 28), with an overall mass loss of 14.

Previous NMR and mass spectrometric studies have also identified the formation of cyclic trimers and higher oligomers in similar systems involving other bridging organic moieties.[29, 30] Based on the mechanistic studies of Shea and Loy,[25] the formation of cyclic oligomers (which reduce condensation and gelation rates by acting as "kinetic bottlenecks" during the sol-gel processing of bridged silsesquioxanes) could presumably be discounted on mechanistic grounds in our system. However, it should be noted that the possible formation of small quantities of such species in our system cannot be completely discounted on the basis of the observed mass spectrometric data alone, although their mass would be expected to exceed 1500.

These observations suggest that the coatings deposited from HCl-catalysed sols are constructed from the assembly of essentially monomeric species formed via transesterification/hydrolysis of the **P12** precursor, whereas coatings obtained from NH_4F-catalysed sols are constructed from polycondensed species with dimensions of 3 to 5 nm. It should be noted that attempts to record the infrared spectra of these species were unsuccessful, due to their relatively low concentration and the correspondingly high intensity of features arising from the solvent.

Nanoscale Organisation and Self-Assembly during Spin-Coating

The observation that polycondensed solution species in the NH_4F-catalysed solutions yield relatively homogeneous and featureless coatings, whereas the hydrolysed monomeric molecular species present in the HCl-catalysed solutions yield coatings with a fibrous morphology is intriguing and counter-intuitive. In the case of the HCl-catalysed system, this suggests

that self-assembly leading to formation of fibres occurs during spin-coating and associated solvent evaporation. This, together with the significantly different morphologies obtained under NH_4F- and HCl-catalysed conditions, suggests that the structural evolution of the corresponding coatings is modulated by both physical and chemical control. To elucidate the processes occurring during formation of the coatings, their structural evolution was probed by vibrational spectroscopy.

The FTIR spectra (ν(C-H) region) of **P12** and coatings deposited from NH_4F- and HCl-catalysed sols, aged for four hours prior to spin-coating at 8000 min^{-1}, are illustrated in Figure 4. The spectrum of **P12** exhibits well-defined bands at 2852, 2883, 2926 and 2974 cm^{-1}, in good agreement with previous reports,[20] which are assigned to $\nu_s(CH_2$, alkyl chain); $\nu_s(CH_3$, alkoxy); $\nu_{as}(CH_2$, alkyl chain) and $\nu_{as}(CH_3$, alkoxy), respectively. The peaks associated with the alkylene chains are retained in the spectra of the films, as expected, while the peaks associated with the ethoxy species are eliminated in the case of the HCl- and NH_4F-catalysed materials, consistent with essentially complete hydrolysis during ageing and/or deposition of the coatings. Note that these latter peaks are still evident in the spectrum of the coating prepared under NH_4OH-catalysed conditions, reflecting incomplete hydrolysis in this case (Supplementary Information, Figure S3). As mentioned before, our studies were thus mainly focused on the NH_4F- and HCl-catalysed films. The position and full-width at half-maximum (FWHM) of the $\nu_{as}(CH_2)$ mode are sensitive to the environment of the alkylene chains,[17] with chains in an all-trans "liquid-crystal" environment giving rise to a peak at 2923 cm^{-1}, while those in a "liquid-like" environment exhibit a mode at 2936 cm^{-1}. In the current work, **P12** and the NH_4F- and HCl-catalysed materials all exhibit a peak near 2926 cm^{-1}, consistent with the alkylene chains adopting an all-trans configuration. However, the peak is significantly broader in the case of the NH_4F-catalysed system, suggesting that the chains are less-ordered than in the case of the HCl-catalysed material. A similar trend is evident in the $\delta(CH_2)$ region (Figure 5), where the mode observed at 1465 cm^{-1}, associated with an all-trans alkylene chain configuration,[17] is significantly broader in the case of the NH_4F-catalysed system.

Non-covalent interactions such as the strength of H-bonding interactions between urea groups in such nanohybrids, can be probed by vibrational spectroscopy in the range from 1500 to 1750 cm^{-1} where amide-1 and amide-2 vibrations dominated respectively by intramolecular ν(C=O) and δ(NH) bands are observed. Generally, self-assembly of bridged silsesquioxanes incorporating urea moieties is mediated by H-bonding between these groups, and both the wavenumber and full-width at half-maximum (FWHM) of the amide-1 mode are sensitive indicators of the strength and homogeneity of intermolecular H-bonding in these materials (with increasing H-bonding strength leading to a corresponding decrease in the wavenumber of the amide-1 mode). Similarly, the separation between the amide-1 and amide-2 modes (Δ) is also a function of the strength of H-bonding, with values of Δ around 40 cm^{-1} reflecting strong H-bonding and values in excess of 100 cm^{-1} typical of non-H-bonded systems.[17, 31-35]

Variations in the positions, relative intensities and full-width at half-maximum (FWHM) of the amide-1 and amide-2 modes for **P12** and the coatings prepared from HCl- and NH_4F-catalysed sols are illustrated in Figures 5 and 6 and Table S1 (Supporting Information). The spectrum of **P12** has been described previously by Moreau et al,[20] who observed peaks at 1577 and 1625 cm^{-1} which were attributed to amide-2 and amide-1, respectively (corresponding to the modes observed in the present work at 1573 and 1620 cm^{-1}, Figure 5). The separation between these peaks (Δ = 47 cm^{-1}) is consistent with strong inter-molecular H-bonding between urea moieties on adjacent **P12** molecules, while the corresponding FWHM (25 and 20 cm^{-1}, respectively) are consistent with a narrow distribution of H-bond energies. Curve fitting experiments (Supplementary Information, Figure S7), confirm that the spectral profile in this region can be well represented by two peaks, consistent with a well-defined, homogeneous network of H-bonds in **P12**.

In contrast, somewhat broader amide-1 and amide-2 band profiles are observed for films produced from **P12** sols prepared under HCl- or NH_4F-catalysed conditions (Figures 5 and 6), consistent with a less homogeneous distribution of H-bonding interaction energies in the coatings. Curve fitting studies revealed the presence of four peaks in each case, as summarised in Table S1 (Supporting Information). Peaks 2 and 3 are attributed to strongly H-bonded moieties ($\Delta_{(2-3)}$ = 46 and 58 cm^{-1} for the HCl- and NH_4F catalysed systems, respectively), while Peaks 1 and 4 are attributed to weakly- or non-H-bonded species ($\Delta_{(1-4)}$ = 99 to 117 cm^{-1}). It is interesting to note that the FWHM for Peaks 1 to 4 in the HCl-catalysed system are all lower than the corresponding modes in the NH_4F-catalysed material by around 10 cm^{-1}, reflecting a more homogeneous distribution of H-bonding energies in the former material. Similarly, $\Delta_{(2-3)}$ and $\Delta_{(1-4)}$ and the wavenumber of the amide-1 modes are lower for the HCl-catalysed system, reflecting stronger H-bond strength in that system (Table S1, Supporting Information). The impact of such non-covalent bonding on the structural evolution of the coatings will be discussed in more detail below.

The impact of spinning speed on the molecular scale organisation in coatings produced from HCl-catalysed sols is illustrated in Table S2 (Supporting Information). Only minor differences are evident in the spectral profiles, suggesting that spinning speed has little impact on the organisation within the coatings on the molecular scale. This is further emphasised by a more detailed analysis of the spectral profiles via curve fitting, as shown in Figure 6. The FWHM and wavenumber of Peaks 2 and 3 (associated with strongly H-bonded species) are essentially constant with changing spinning speed, indicating that self-assembly is independent of spinning speed and is controlled by chemical interactions rather than physical parameters such as evaporation rate. In contrast, the FWHM of Peak 1 decreases with increasing spinning speed, consistent with a decrease in the heterogeneity of H-bonding energies in these weakly bonded sites. A corresponding, albeit smaller, decrease in the FWHM of Peak 4 with increasing spinning speed is also evident. An analysis of the integrated band intensities of Peaks 1 and 2 reveals an increase in the intensity

of Peak 2 relative to Peak 1 with increasing spinning speed, suggesting that weakly H-bonded species are converted to strongly H-bonded species with increasing spinning speeds. This conversion is presumably the origin of the decrease in the heterogeneity of H-bonding energies of the former species with increased spinning speed.

Further insights into the molecular-scale organisation within the coatings produced from HCl-catalysed sols are obtained via the use of polarised IR light to probe the orientation of the –NH and –CO species. Figure 7 illustrates the polarised IR spectra of coatings deposition under HCl-catalysed conditions as a function of spinning speed, while the corresponding peaks parameters obtained via curve fitting are summarised in Table S3 (Supporting Information). Significant differences are evident between the spectra recorded under horizontally- and vertically-polarised conditions, with the relative intensities of Peaks 1 and 4 (associated with weakly H-bonded species) being significantly stronger under vertically-polarised conditions. This observation is further emphasised by comparing the ratio of the integrated intensities of Peaks 1 and 2 under different polarisation conditions (Table S3, Supporting Information), with I_2/I_1 being consistently smaller in vertical polarisation as compared to horizontal polarisation. This suggests that the strongly H-bonding species promoting self-assembly and formation of a fibrous morphology in this system are predominantly oriented horizontal to the substrate, while the weakly H-bonded species are predominantly orientated vertical to the substrate. No consistent trends are evident with respect to spinning speed, once again highlighting the role of chemical parameters rather than physical parameters in mediating self-assembly. In particular, this suggests that the timescales over which the H-bond networks form and adopt their preferred orientation is short compared to the timescale imposed by the spin-coating process (which controls evaporation rates and concentration profiles within the evolving coatings).

The sensitivity of the inorganic network to spinning speed was further studied by investigating the response of the Si-O-Si antisymmetric stretching modes (transverse optic (TO) component) to spinning speed via infrared spectroscopy.[17] Here we performed an ATR study using the silicon wafer substrate as a waveguide for the infrared light. Spectra are shown (Figure S8, supplementary information) for spinning speeds of 3000 and 5000 min^{-1}. Note that characterization of the Si-O-Si antisymmetric stretching modes is not possible in either transmission or ATR using a diamond crystal waveguide, due to the absorbance of the silicon wafer substrate in this region (1200 – 600 cm^{-1}). The high intensity of the most prominent Si-O-Si antisymmetric stretching band [36] around 1021 cm^{-1} relative to the slope around 1150 cm^{-1} suggests the predominance of open-chain polymeric siloxane (ladder-like oligomers) species in the films. The comparison of the infrared features as a function of the spinning speed suggests a less-condensed system at low spinning speeds. The lower rate of condensation appears to be correlated to the presence of longer fibres, possibly due to more extensive self-assembly of the organics in the film.

Proposed Mechanism

On the basis of the results presented above, a mechanism for the formation of coatings from NH_4F- and HCl-catalysed sols is proposed in Figure 8. The initiation of sol-gel chemistry in solutions under HCl-catalysed conditions generates hydrolysed species, although no significant polycondensation is evident even after ageing for 24 hours. In contrast, sols produced under NH_4F-catalysed conditions exhibited significant polycondensation after ageing for four hours, reflecting fundamental differences in the structure of the "building blocks" from which coating will subsequently be constructed.

The subsequent formation of coatings from the respective sols via spin-coating and rapid spreading and concentration of the surface layer yields significantly different coating morphologies, due to the different building blocks involved in the structural evolution of the coatings. Spin coating in such complex systems is a highly non-equilibrium process, with rapid increases in reactant concentration interacting with nucleation, growth, self-assembly and polycondensation processes during formation of the coating. This indicates that the time available for the solution species to react during coating deposition is short, and non-equilibrium structures would be expected to be "frozen" in place.

In the case of HCl-catalysed sols, condensation (promoted by a rapid decrease in pH during evaporation) and self-assembly both proceed during coating deposition, yielding a fibrous morphology. The spectroscopic data indicate that the fibres are characterised by the presence of a network of strong and energetically homogeneous H-bonds, and the uniform structures obtained suggest that self-assembly via H-bonding occurs initially, followed by inorganic polycondensation. The weaker and energetically inhomogeneous H-bonds also observed in the HCl-catalysed system might arise from bonding between the individual fibres. The observation (from AFM and SEM) that increasing spinning speed leads to a corresponding decrease in the size of the holes in the fibrous net, and to a much tighter structure, suggests that the formation of the fibres in the concentrated solution film occurs on a much shorter time scale than the spinning-induced evaporation and concentration of the species in solution. The decrease in the average length of the fibres with increasing spinning speed is attributed to variations in the relative rates of nucleation and growth with spinning speed.[37] In particular, at higher spinning speeds (with a correspondingly higher supersaturation of reactants), nucleation would be expected to dominate growth, leading to a greater number of small fibres. In contrast, at lower spinning speeds (and lower reactant supersaturation), growth would be expected to dominate nucleation, leading to a smaller number of larger fibres. The decrease in roughness with increasing spinning speed (Figure 2) is consistent with more uniform packing of the fibres formed during the initial stages of the spin-coating process.

A key feature of the mechanism proposed above is the rapid template-free self-structuring process occurring during spin-

coating. Such "evaporation-induced self-structuring" (EISS) is phenomenologically similar to the interplay between self-assembly and solvent evaporation that occurs during evaporation-induced self-assembly (EISA) in dip-coating,[38, 39] where the increasing concentration of reactants during dip-coating drives surfactant self-assembly to form a template around which inorganic polycondensation of small, flexible inorganic building blocks subsequently occurs. In the present case, the time-scales imposed by the spin-coating process are much shorter than those in EISA (seconds vs minutes), suggesting that kinetic control of self-structuring occurs in EISS compared to thermodynamic control in the case of EISA. In contrast, in the case of the NH_4F-catalysed system, polycondensation occurs prior to formation of the coating layer (as shown by dynamic light scattering), generating small, relatively rigid species in solution that would not be sufficiently flexible to generate the extended, uniform H-bonded networks that are evident in the HCl-catalysed system. This expectation is evident both in the spectroscopic data (which indicate that the H-bonds in this system are less ordered and typically weaker) and AFM/SEM data (which are consistent with the absence of extended self-assembled networks). The role of the relatively rigid, partially-condensed species in suppressing the formation of extended self-assembled networks in the NH_4F-catalysed system is consistent with the proposed mechanism for the HCl-catalysed system, namely that self-assembly occurs before extensive inorganic polycondensation.

The relatively narrow processing windows that can be used to produce high quality coatings, particularly in the HCl-catalysed system, can also be interpreted on the basis of the proposed model. Although no polycondensed species are evident in the HCl-catalysed system for ageing times of up to 24 hours, the mass spectrometry data clearly indicates that hydrolysis and transesterification continue, yielding a variety of hydroxylated species that would be expected to participate in H-bonding interactions with the amide sites which facilitate self-assembly. Increasing extent of hydroxylation (associated with an increasing probability of ≡Si–O…H-N-C… and ≡Si–OH…O=C… interactions) would be expected to result in increasing disruption of the urea-urea network, thus disrupting the self-assembly process mediating film formation. This expectation was confirmed by IR spectroscopy for coatings deposited from sols aged for 24 hours, where a significant increase in the FWHM of the amide-1 band profile centred at 1623 cm^{-1} was clearly observed. Deconvolution of this band profile reveals a six-fold increase in the intensity of Peak 1 relative to that of Peak 2 with ageing (Supplementary Information, Table S4), together with an increase in the FWHM of Peak 1. This is attributed to an increase in the abundance of weakly H-bonded species in the coating and/or to an increase in the heterogeneity of H-bond energies.

Conclusions

The use of Evaporation-Induced Self-Structuring (EISS) as a general approach for producing organised nanohybrid coatings from multifunctional precursors via spin coatings is exemplified. Spin-coating is a highly non-equilibrium process, and exploiting the cooperative interactions between chemical parameters (which control the structure of "building blocks" formed in sol-gel solutions prior to deposition of the coatings) and physical parameters provides new approaches for controlling the structural evolution of thin films. In particular, the template-free EISS approach is mediated by rapid evaporation of the solvent within seconds, providing kinetic control of self-structuring. In contrast structuring of micelle-silicates composites in alternative approaches such as EISA occurs over significantly longer timescales (typically minutes).

This approach is demonstrated using 1,12-bis[(triethoxysilyl)-propylureido] dodecane as a precursor for depositing nano-patterned films by spin-coating from pre-hydrolysed solutions produced under NH_4F- or HCl-catalysed conditions. Spin-coating of these sols, where rapid increases in reactant concentration interact with nucleation, growth, self-assembly and polycondensation during formation of the coating, yields significantly different morphologies due to the short time scales (seconds) available for the solution species to react during deposition and the associated "immobilisation" of non-equilibrium structures. For example, in the case of HCl-catalysed sols, condensation (promoted by a rapid decrease in pH during evaporation) and self-assembly both proceed during coating deposition, yielding a fibrous morphology. Spectroscopic data indicate that the molecular species present in the pre-hydrolysed solutions self-assemble to form fibres during the initial stages of film formation (rapid evaporation of the solvent), followed by inorganic polycondensation to produce a gel network. The generalisation of this concept to functional organosilanes should lead to better control of the thin-film nanostructures produced during coating deposition, and hence to improved properties for a variety of applications.

Acknowledgements

Western Sydney University (IRIS grant), the University of Montpellier, ENSCM and CNRS are gratefully acknowledged for funding. We thank Guillaume Cazals (IBMM, Montpellier), Didier Cot (IEM, Montpellier), Michel Ramonda (L2C, Montpellier); Marine Liotaud (Inst. Néel, Grenoble) and Bernard Fraisse (ICG Montpellier) for their help in thin films characterisations.

Notes and references

1 1. K. J. S. Shea, D. A. Loy and O. W. Webster, *Chem. Mater.*, 1989, **1**, 572-574.
2 2. R. J. P. Corriu, J. J. E. Moreau, P. Thépot and M. Wong Chi Man, *Chem. Mater.*, 1992, **4**, 1217-1224.
3 3. A. Chemtob, L. Ni, C. Croutxé-Barghorn and B. Boury, *Chem. Eur. J.*, 2014, **20**, 1790-1806.
4 4. C. Sanchez, C. Boissière, D. Grosso, C. Laberty and L. Nicole, *Chem. Mater.*, 2008, **20**, 682-737.
5 5. C. Sanchez, P. Belleville, M. Popall and L. Nicole, *Chem. Soc. Rev.*, 2011, **40**, 696-753.

6 6. N. G. Liu, K. Yu, B. Smarsly, D. R. Dunphy, Y. B. Jiang and C. J. Brinker, *J. Am. Chem. Soc.*, 2002, **124**, 14540-14541.
7 7. P. N. Minoofar, R. Hernandez, S. Chia, B. Dunn, J. I. Zink and A.-C. Franville, *J. Am. Chem. Soc.*, 2002, **124**, 14388-14396.
8 8. H. R. Li, L. S. Fu, J. Lin and H. J. Zhang, *Thin Solid Films*, 2002, **416**, 197-200.
9 9. B. Lei, B. Li, H. Zhang, S. Lu, Z. Zheng, W. Li and Y. Wang, *Adv. Funct. Mater.*, 2006, **16**, 1883-1891.
10 10. S. Tao, G. Li and H. Zhu, *J. Mater. Chem.*, 2006, **16**, 4521-4528.
11 11. J. Graffion, A. M. Cojocariu, X. Cattoen, R. A. S. Ferreira, V. R. Fernandes, P. S. Andre, L. D. Carlos, M. Wong Chi Man and J. R. Bartlett, *J. Mater. Chem.*, 2012, **22**, 13279-13285.
12 12. C. Urata, B. Masheder, D. F. Cheng, D. F. Miranda, G. J. Dunderdale, T. Miyamae and A. Hozumi, *Langmuir*, 2014, **30**, 4049-4055.
13 13. V. T. Freitas, L. Fu, A. M. Cojocariu, X. Cattoën, J. R. Bartlett, R. Le Parc, J.-L. Bantignies, M. Wong Chi Man, P. S. André, R. A. S. Ferreira and L. D. Carlos, *ACS Appl. Mater. Interfaces*, 2015, **7**, 8770-8778.
14 14. J. J. E. Moreau, L. Vellutini, M. Wong Chi Man, C. Bied, J. L. Bantignies, P. Dieudonné and J. L. Sauvajol, *J. Am. Chem. Soc.*, 2001, **123**, 7957-7958.
15 15. J. J. E. Moreau, B. P. Pichon, C. Bied and M. Wong Chi Man, *J. Mater. Chem.*, 2005, **15**, 3929-3936.
16 16. J. J. E. Moreau, B. P. Pichon, M. Wong Chi Man, C. Bied, H. Pritzkow, J. L. Bantignies, P. Dieudonné and J. L. Sauvajol, *Angew. Chem. Int. Ed.*, 2004, **43**, 203-206.
17 17. J. L. Bantignies, L. Vellutini, D. Maurin, P. Hermet, P. Dieudonné, M. Wong Chi Man, J. R. Bartlett, C. Bied, J. L. Sauvajol and J. J. E. Moreau, *J. Phys. Chem. B*, 2006, **110**, 15797-15802.
18 18. A. Chemtob, L. Ni, C. Croutxé-Barghorn, A. Demarest, J. Brendlé, L. Vidal and S. Rigolet, *Langmuir*, 2011, **27**, 12621-12629.
19 19. I. Karatchevtseva, D. J. Cassidy, M. Wong Chi Man, D. R. G. Mitchell, J. V. Hanna, C. Carcel, C. Bied, J. J. E. Moreau and J. R. Bartlett, *Adv. Funct. Mater.*, 2007, **17**, 3926-3932.
20 20. J. J. E. Moreau, L. Vellutini, M. Wong Chi Man, C. Bied, P. Dieudonné, J. L. Bantignies and J. L. Sauvajol, *Chem. Eur. J.*, 2005, **11**, 1527-1537.
21 21. W. Kern, *J. Electrochem. Soc.*, 1990, **137**, 1887-1892.
22 22. D. A. Loy, K. A. Obrey-DeFriend, K. V. Wilson Jr, M. Minke, B. M. Baugher, C. R. Baugher, D. A. Schneider, G. M. Jamison and K. J. Shea, *J. Non-Cryst. Solids*, 2013, **362**, 82-94.
23 23. L.-C. Hu and K. J. Shea, *Chem. Soc. Rev.*, 2011, **40**, 688-695.
24 24. D. W. Schaefer, G. Beaucage, D. A. Loy, K. J. Shea and J. S. Lin, *Chem. Mater.*, 2004, **16**, 1402-1410.
25 25. K. J. Shea and D. A. Loy, *Acc. Chem. Res.*, 2001, **34**, 707-716.
26 26. K. Norrman, A. Ghanbari-Siahkali and N. B. Larsen, *Annu. Rep. Prog. Chem., Sect. C: Phys. Chem.*, 2005, **101**, 174-201.
27 27. S. Guo, A. Sugawara-Narutaki, T. Okubo and A. Shimojima, *J. Mater. Chem. C*, 2013, **1**, 6989-6995.
28 28. R. Pecora, *J. Nanopart. Res.*, 2000, **2**, 123-131.
29 29. L. Gabrielli, L. Russo, A. Poveda, J. R. Jones, F. Nicotra, J. Jiménez-Barbero and L. Cipolla, *Chem. Eur. J.*, 2013, **19**, 7856-7864.
30 30. A. A. Letailleur, F. Ribot, C. Boissière, J. Teisseire, E. Barthel, B. Desmazières, N. Chemin and C. Sanchez, *Chem. Mater.*, 2011, **23**, 5082-5089.
31 31. J. Jadzyn, M. Stockhausen and B. Zywucki, *J. Phys Chem.*, 1987, **91**, 754-757.
32 32. J. vanEsch, R. M. Kellogg and B. L. Feringa, *Tetrahedron Lett.*, 1997, **38**, 281-284.
33 33. P. Ribagnac, C. Cannizzo, R. Méallet-Renault, G. Clavier, P. Audebert, R. Pansu and L. Bouteiller, *J. Phys. Chem. B*, 2013, **117**, 1958-1966.
34 34. B. Isare, G. Pembouong, F. Boué and L. Bouteiller, *Langmuir*, 2012, **28**, 7535-7541.
35 35. G. Creff, B. P. Pichon, C. Blanc, D. Maurin, J.-L. Sauvajol, C. Carcel, J. J. E. Moreau, P. Roy, J. R. Bartlett, M. Wong Chi Man and J.-L. Bantignies, *Langmuir*, 2013, **29**, 5581-5588.
36 36. Z. Zhang, H. Wakabayashi and T. Akai, *J. Sol-Gel Sci. Technol.*, 1998, **12**, 153-158.
37 37. V. Monnier, N. Sanz, E. Botzung-Appert, M. Bacia and A. Ibanez, *J. Mater. Chem.*, 2006, **16**, 1401-1409.
38 38. A. Gibaud, D. Grosso, B. Smarsly, A. Baptiste, J. F. Bardeau, F. Babonneau, D. A. Doshi, Z. Chen, C. J. Brinker and C. Sanchez, *J. Phys. Chem. B*, 2003, **107**, 6114-6118.
39 39. L. Nicole, C. Boissiere, D. Grosso, A. Quach and C. Sanchez, *J. Mater. Chem.*, 2005, **15**, 3598-3627.
40

Scheme 1. Production of thin films from P12 precursor

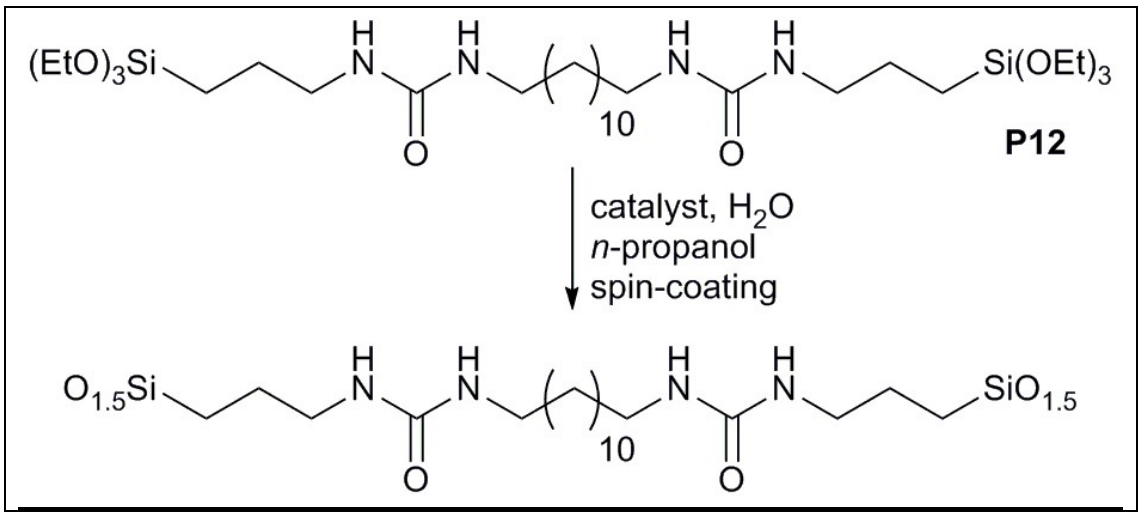

Figure 1. AFM micrographs of coatings produced under (a) HCl- and (b) NH_4F-catalysed conditions (Coating conditions: 1 % P12 in 1-PrOH; Si:H_2O = 1:23; ageing time = 4 h; spinning speed=8000 min^{-1} for 60 s). The micrograph of the coating deposited from NH_4F-catalysed sol is shown at higher resolution (5×5 μm) than that deposited from HCl-catalysed sol (10×10 μm)

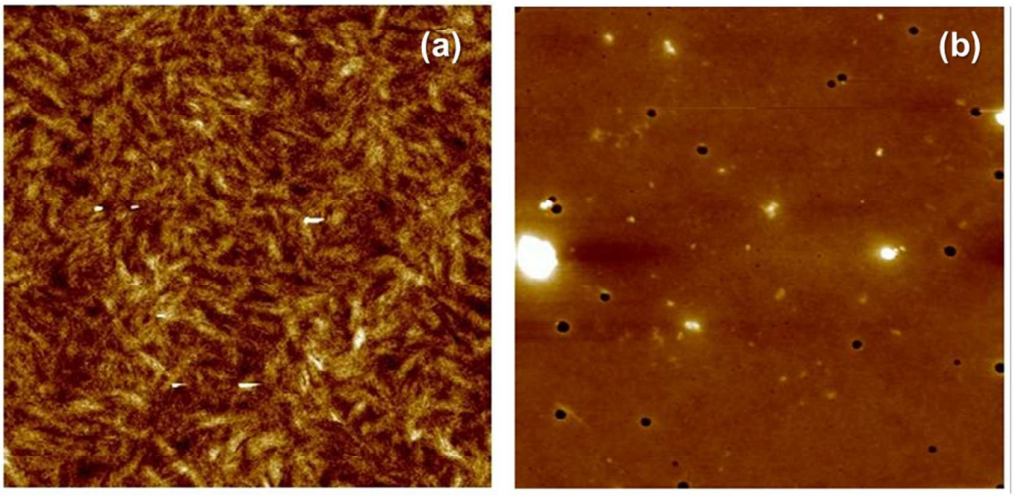

Figure 2. Variations in the AFM (top, 10×10 μm, 2 μm bar) and SEM micrographs (bottom, 1 μm bar) of coatings produced under HCl-catalysed conditions as a function of spinning speed. (Coating conditions: 1 % **P12** in 1-PrOH; Si:H_2O = 1:23; ageing time = 4 h; spinning speed= (a) 8000; (b) 5000; (c) 3000; and (d) 1000 min^{-1} for 60 s. The coating roughness, R_a, and average fibre length, L, are shown in each case).

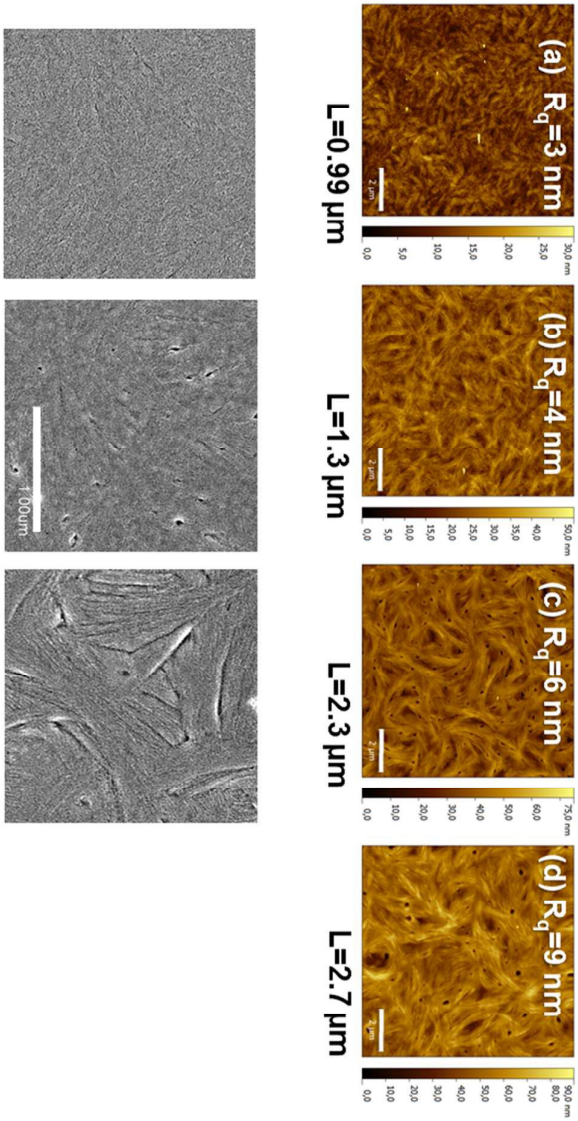

Figure 3. Variations in hydrodynamic radii (from dynamic light scattering) with ageing time in sols produced under NH_4F- and HCl-catalysed conditions.

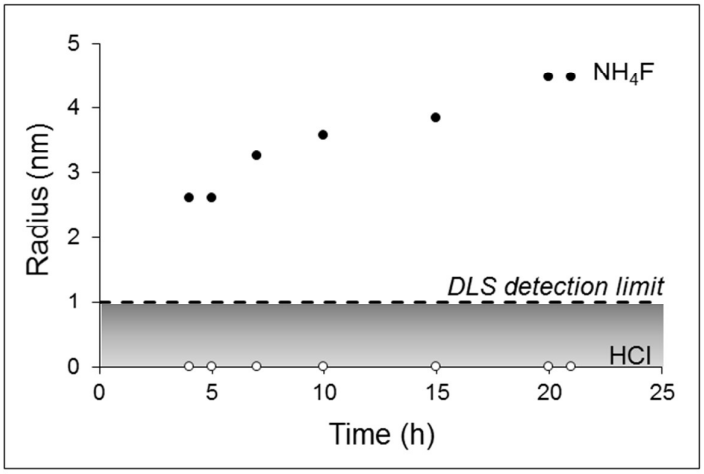

Figure 4. Middle infrared spectra in the region of νCH of **P12** and films produced from sols prepared using HCl or NH_4F as catalyst (Conditions: 1 % **P12** in 1-PrOH; Si:H_2O = 1:23; ageing time = 4 h; spinning speed = 8000 min^{-1} for 60 s).

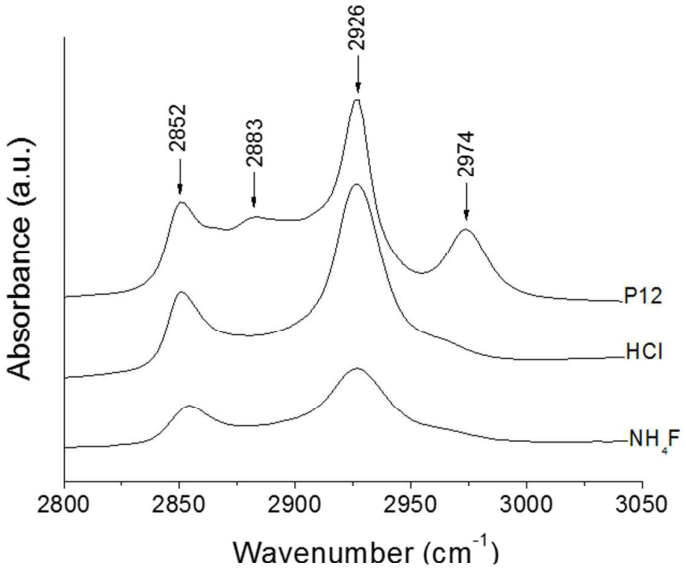

Figure 5. Middle infrared spectra in the region of δCH and amide 1 and 2 of **P12** and films produced from sols prepared using HCl, or NH_4F as catalyst (Conditions for depositing coatings: 1 % P12 in 1-PrOH; Si:H_2O = 1:23; ageing time = 4 h; spinning speed = 8000 min^{-1} for 60 s).

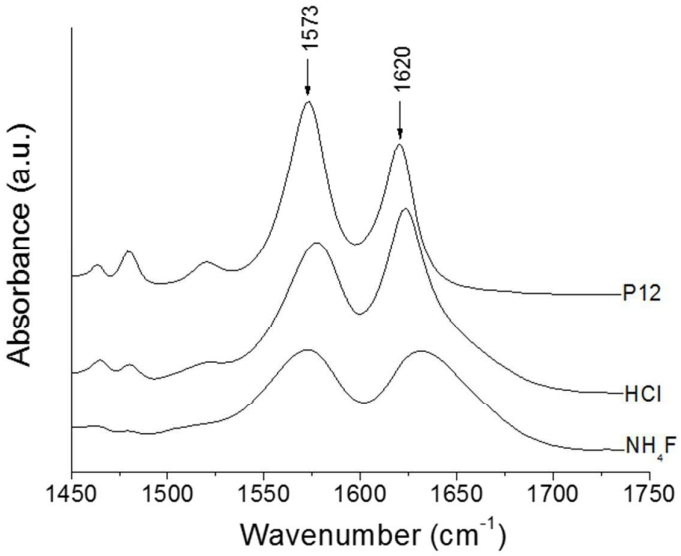

Figure 6. *Top*: FWHM of amide-1 and amide-2 peaks in the spectra of **P12** and coatings prepared from HCl- and NH_4F-catalysed sols (Conditions for depositing coating: 1 % **P12** in 1-PrOH; Si:H_2O = 1:23; ageing time = 4 h; spinning speed=8000 min^{-1} for 60 s).

Bottom: Effect of spin-coating speed on the FWHM of amide-1 and amide-2 band profiles for coatings prepared from HCl-catalysed sols.

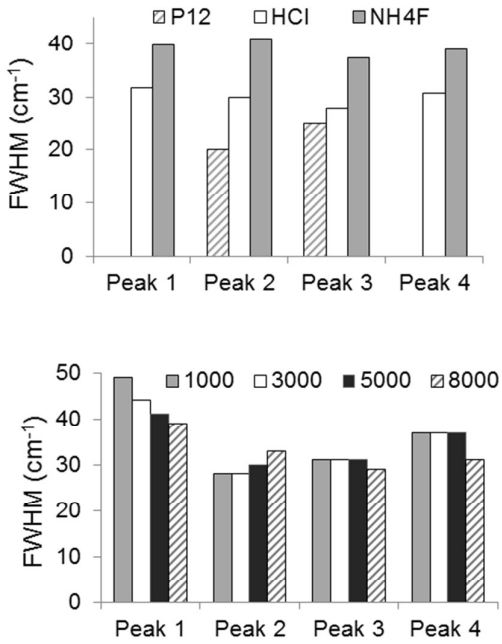

Figure 7. Infrared spectra of coatings deposited from HCl-catalysed sols using horizontally- (H) or vertically-polarised light (V), as a function of spinning speed. (Conditions for depositing coating: 1 % **P12** in 1-PrOH; Si:H_2O = 1:23; ageing time = 4 h; spinning speed=1000, 3000, 5000 or 8000 min^{-1} for 60 s).

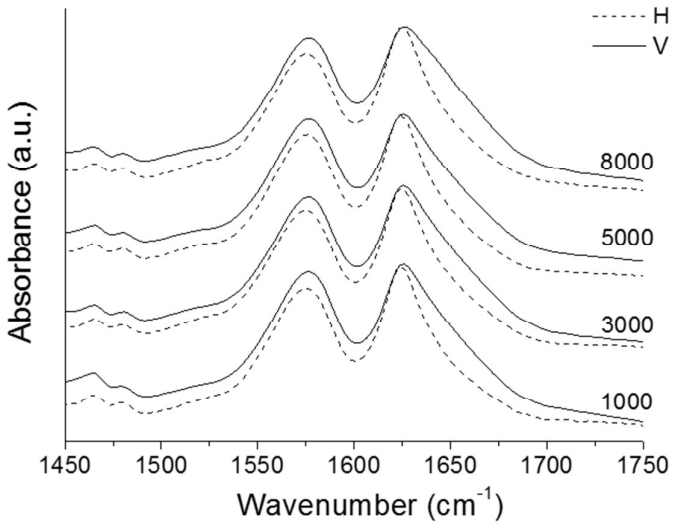

Figure 8. Proposed mechanism for the formation of coatings under HCl- (Top) and NH_4F-catalysed conditions (Bottom). R = H, CH_3-CH_2 or CH_3-CH_2-CH_2.

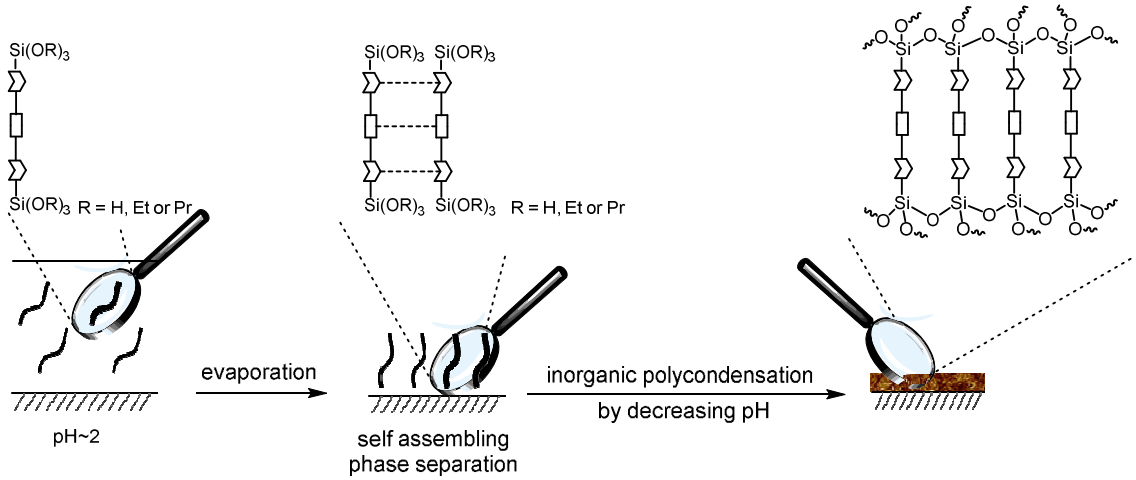

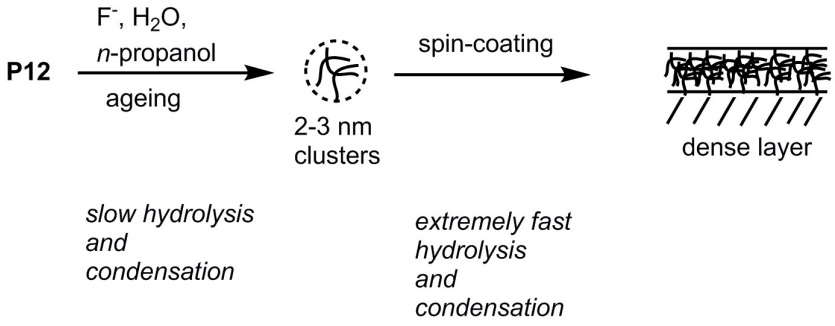

Table of Contents Graphic